European Polymer Journal 141 (2020) 110070

Contents lists available at ScienceDirect

European Polymer Journal

journal homepage: www.elsevier.com/locate/europolj

Boosting up printability of biomacromolecule based bio-ink by modulation of hydrogen bonding pairs

Busra Koksal[a], Rabia Onbas[b], Mehmet Baskurt[c], Hasan Sahın[c], Ahu Arslan Yildiz[b,*], Umit Hakan Yildiz[a,c,d,*]

[a] Department of Chemistry, Izmir Institute of Technology, 35430 Urla, İzmir, Turkey
[b] Department of Bioengineering, Izmir Institute of Technology, 35430 Urla, İzmir, Turkey
[c] Department of Photonics, Izmir Institute of Technology, 35430 Urla, İzmir, Turkey
[d] Department of Polymer Science and Engineering, Izmir Institute of Technology, 35430 Urla, İzmir, Turkey

ARTICLE INFO

Keywords:
Hydrogel
Bioink
Bioprinting
3D Scaffold
Gelatin
Tissue engineering

ABSTRACT

This study describes low dose UV curable and bioprintable new bioink made of hydrogen bond donor-acceptor adaptor molecule 2-isocyanatoethyl methacrylate (NCO)modified gelatin (NCO-Gel). Our theoretical calculations demonstrate that insertion of 2-isocyanatoethyl methacrylate doubles the interaction energy (500 meV) between gelatin chains providing significant contribution in interchain condensation and self-organization as compared to methacrylic anhydride modified gelatin (GelMA). The NCO-Gel exhibits peak around 1720 cm^{-1} referring to bidentate hydrogen bonding between H-NCO and its counterpart O═CN—H. These strong interchain interactions drive chains to be packed and thereby facilitating UV crosslinking. The NCO-Gel is exhibiting a rapid, 10 s gelation process by the exposure of laser (3 W, 365 nm). The dynamic light scattering characterization also reveals that NCO-Gel has faster sol to gel transition as compared to GelMA depending on the UV curing time. The NCO-Gel was found to be more firm and mechanically strong that provides advantages in molding as well as bioprinting processes. Bioprinted NCO-Gel has shown sharp borders and stable 3D geometry as compared to GelMA ink under 10 s UV curing time. The cell viability tests confirm that NCO-Gel facilitates cell proliferation and supports cell viability. We foresee that NCO-Gel bioink formulation provides a promising opportunity when low dose UV curing and rapid printing are required.

1. Introduction

Biofabrication of suitable biomaterials for applications in biotechnology and biomedicine requires several aspects such as mimicking the nature of original tissues and compatibility to tissues. Hydrogels emergeas good candidates for such applications by their excellent biocompatibility, functionality, responsiveness and excellent chemical and physical properties. They are highly preferred in many fields like biomedicine, pharmaceutical industry, biotechnology and tissue engineering [1–4] as therapeutic agent delivery systems [5–7], biosensors [8–10], diagnostic and imaging tools [11–13] and tissue scaffolds [14–16] for many tissue and organ models. Recently we summarize the properties and applications of biomimetic and synthetic hydrogels that provide general perspective for hydrogel based materials [17]. A major challenges for hydrogels in 3D bioprinting has been extensively encountered for instance; arranging cells, functionalization of biologically active factors for multilayer fabrication of artificial tissue models [18–24]. Bertassoni et al. achieved bioprinting of cell-laden gelatinmethacrylamide (GelMA) bioinks for fabrication of 3D constructs containing hepatocyte and fibroblast cells. Printability of GelMA hydrogels mainly depends on concentration of GelMA bioink. Below 7% GelMA, printing process has not been achieved. Whereas the cell density and UV exposure time affect the reproducibility of the printing, they produced 3D constructs using 10% GelMA showing good cell viability and proliferation [25]. To improve the printability of gelatin based materials, Skardal et al. synthesized methacrylatedethanolamide derivative of gelatin (GE-MA) and methacrylated hyaluronic acid (HA-MA) hydrogels as bioink. They printed the polymer bioink at tubular geometry with good mechanical properties and enough sites for cell attachments. But the printed tubular structures had thick walls and not interconnected pores which should be improved [26]. Shin et al. developed a conductive bioink including GelMA, deoxyribonucleic acid

* Corresponding authors at: Department of Chemistry, Izmir Institute of Technology, 35430 Urla, İzmir, Turkey (Ü.H. Yildiz). Department of Bioengineering, Izmir Institute of Technology, 35430 Urla, İzmir Turkey (A. Arslan Yildiz).
E-mail addresses: ahuarslan@iyte.edu.tr (A. Arslan Yildiz), hakanyildiz@iyte.edu.tr (U.H. Yildiz).

https://doi.org/10.1016/j.eurpolymj.2020.110070
Received 31 July 2020; Received in revised form 26 September 2020; Accepted 28 September 2020
Available online 06 October 2020

(DNA) and carbon nanotube (CNT) as an applications for wearable electronics. The printed constructs showed high flexibility and conductivity even if the construct were folded, bent, or stretched [27]. Weitao et al. fabricated a cell-responsive bioink with GelMA, sodium alginate, and 4-arm poly (ethylene glycol)-tetra-acrylate (PEGTA) as well as HUVECs and human mesenchymal stem cells (MSCs). The bioprinted scaffold was crosslinked in two steps as ionic crosslinking of alginate and covalent photocrosslinking of GelMA and PEGTA. The removal of alginate from the scaffold gives vascular channels showing the applicability of the proposed scaffold as blood vessel mimics [21]. Skardal et al. bioprinted amniotic fluid-derived stem cells (AFS) and bone marrow-derived mesenchymal stem cells (MSCs) within fibrin-collagen hydrogel as wound healer and skin regenerative scaffold. Whereas AFS cell and MSCs treated wounds formed ordered epidermal layer and high re-epithelialization on a mice model, the printed cells did not observed in regenerating tissue [28]. In another interesting approach, Kang et al. developed a 3D bioprinter system named as; integrated tissue–organ printer (ITOP) for designing of human scale tissue constructs using cell carrier material; a mixture of gelatin, fibrinogen, HA, glycerol, PCL, tricalcium phosphate (TCP), and Pluronic F127 as bioink. The printed calvarial bone model was implanted into Spraque Dawley rats with bone defects and vascularized bone tissue was formed with blood vessels in the implants treated with bioprinted scaffold as compared with nontreated tissue [29]. Also, Yin et al. mixed GelMA with gelatin to increase the printability and biocompatibility of GelMA as a bioink. Without gelatin, GelMA could not be printed below 15% (w/v), while 2% gelatin/10%GelMA bioink printed. Some compositions of the bioink were not extrudable like 10% gelatin/10% GelMA. The obtained scaffold of 5/8% GelMA/gelatin showed good cell viabilities of Bone marrow stem cells (BMSCs) [30]. Levato et al. utilized a bioink of GelMA hydrogels cultured with articular cartilage-resident chondroprogenitor cells (ACPCs), bone marrow mesenchymal stromal cells (MSCs) and chondrocytes for cartilage regeneration. All cell lines were proliferated in bioprinted zonal-like constructs, they differentiated and produced cartilage matrix on the scaffold after long-term culture. In the study, the mechanical strength of the hydrogel should be increased to that of adult articular cartilage [31]. In overall, high water solubility and easy modification of gelatin leads the scientist to modify gelatin with different chemical strategies and obtain a variety of gelatin-based polymers and hydrogels for tissue engineering applications. One of the most commonly used methods is chain growth polymerization. The obtained material undergoes photocrosslinking with only suitable initiator without any other crosslinker. Gelatin is modified with different functional groups like acrylic anhydride [32], PEG-acrylate moiety [33] and a benzophenone group [34] to increase photocrosslinkable groups on the polymer backbone. The several modification strategies attempt to increase the photocrosslinking ability, mechanical properties and biocompatibility of gelatin-based hydrogels. The bioink, printed material, should mimic the nature of native tissues. GelMA was found to be main component of bioink materials to hold cells and other additives to provide convenient structure and function of scaffold. A functional bioink hydrogels should be printable and protect its printed structure. However methacrylic anhydride modification of gelatin exhibits two major drawbacks i) retention in gelation which limits precision printing ii) low mechanical strength that effect structural integrity of resultant tissues. On the other hand, Kim et al. synthesized silk hydrogels using silk fibroin modified with 2-isocyanatoethyl methacrylate. The photocrosslinking and gelation time of silk fibroin methacrylate was observed as very short time between 39 and 58 s depending on the modification degree. The obtained silk methacrylate hydrogels showed high elasticity. The biocompatibility, high elasticity and fast gelation times of silk fibroin methacrylate hydrogels make them a suitable material for further uses in 3D printing and other biomedical applications [35]. Jung et al. reviewed advantages of light sensitive materials and techniques for designing of 2D, 3D and 4D materials. 3D and 4D printed materials made of stimuli responsive polymer have been fabricated by light mediated printing processes. Fabricated materials have exhibited unique properties such as mimicking the natural tissues and organs, good biocompatibility and high mechanical properties, thanks to spatio-temporal control of light during printing process [36].

In this study we describe modification of gelatin with 2-isocyanatoethyl methacrylate (NCO) that serves as low dose UV curable and bioprintable new bioink. Our theoretical calculations demonstrate that insertion of 2-isocyanatoethyl methacrylate doubles the interaction energy (500 meV) between gelatin chains providing significant contribution in interchain condensation and self-organization as compared to methacrylic anhydride modified gelatin (GelMA). Our postulation is that strong interchain interactions drive chains to be packed and thereby facilitating UV crosslinking. The NCO-Gel was found to be more firm and mechanically strong that provides advantages in molding as well as bioprinting processes. We foresee that NCO-Gel bioink formulation provides a promising opportunity when low dose UV curing and rapid printing are required.

2. Experimental

2.1. Materials

Gelatin (Type A, 225 bloom from porcine skin) was purchased from Bioshop. Methacrylic anhydride (MA), 2-Isocyanatoethyl methacrylate (NCO), 2-Hydroxy-4′-(2-hydroxyethoxy)-2-methylpropiophenone (Irgacure 2959) and Dimethyl sulfoxide (DMSO) were purchased from Sigma Aldrich. UVP CL 1000 UV crosslinker with 365 nm wavelength tubes were used for fabrication of hydrogels. NIH 3T3 mouse fibroblast cells were purchased from ATCC, CRL-1658, DMEM, L-Glutamine, 10% FBS and 1% penicillin/streptomycin were purchased from GIBCO, Thermo Fisher Scientific. MTT reagent; thiazolyl blue tetrazolium bromide was obtained from Sigma Aldrich, and Live/Dead reagents; CytoCalcein™ Green and Propidium Iodide (PI) were obtained from AAT Bioquest. All chemicals were used as received.

2.2. Synthesis of NCO-Gel polymer

Gelatin was modified with 2-isocyanatoethyl methacrylate (NCO) with different modification degrees. The modification process of gelatin is represented in Fig. 2A. Basically, 1 g gelatin (1g) was dissolved in DMSO (27 ml) at 50 °C. While stirring, NCO was added slowly in the amount shown in Table 1. The reaction was allowed to proceed for 6 h at 50 °C under the nitrogen atmosphere. The white solid product was precipitated with the addition of an excess amount of cold isopropanol to the reaction solution. This solution was centrifuged (2000 rpm, 5–10 min). By pipetting solvent phase at top of the solid NCO-Gel solid product was decanted. The white solid was freezed at −80 °C for several hours and lyophilized for 1 day. The produced polymer is named as NCO-Gel. The lyophilized polymer is stored at −80 °C to protect from light and moisture until use.

2.3. Synthesis of GelMA polymer

GelMA polymer was synthesized using the protocol [37] with minor changes. Table 1 shows the composition of GelMA polymers. Briefly, gelatin (1 g) is dissolved in ultrapure water (10 ml) at 45 °C. Predetermined amount of Methacrylic anhydride (MA) was added to the solution and the reaction was allowed to proceed for 3 h at 45 °C under the nitrogen atmosphere. The reaction was finished by diluting the synthesis solution with three volumes of preheated (45 °C) UltraPure water. The resulting solution was put into −80 °C and freezed for several hours. After that, the frozen reaction solution was lyophilized until the polymer was fully dehydrated (2–3 days). The produced polymer is named as Gelatin methacryloyl, GelMA as shortly. GelMA powder was stored at −80 °C to protect from light and moisture until use.

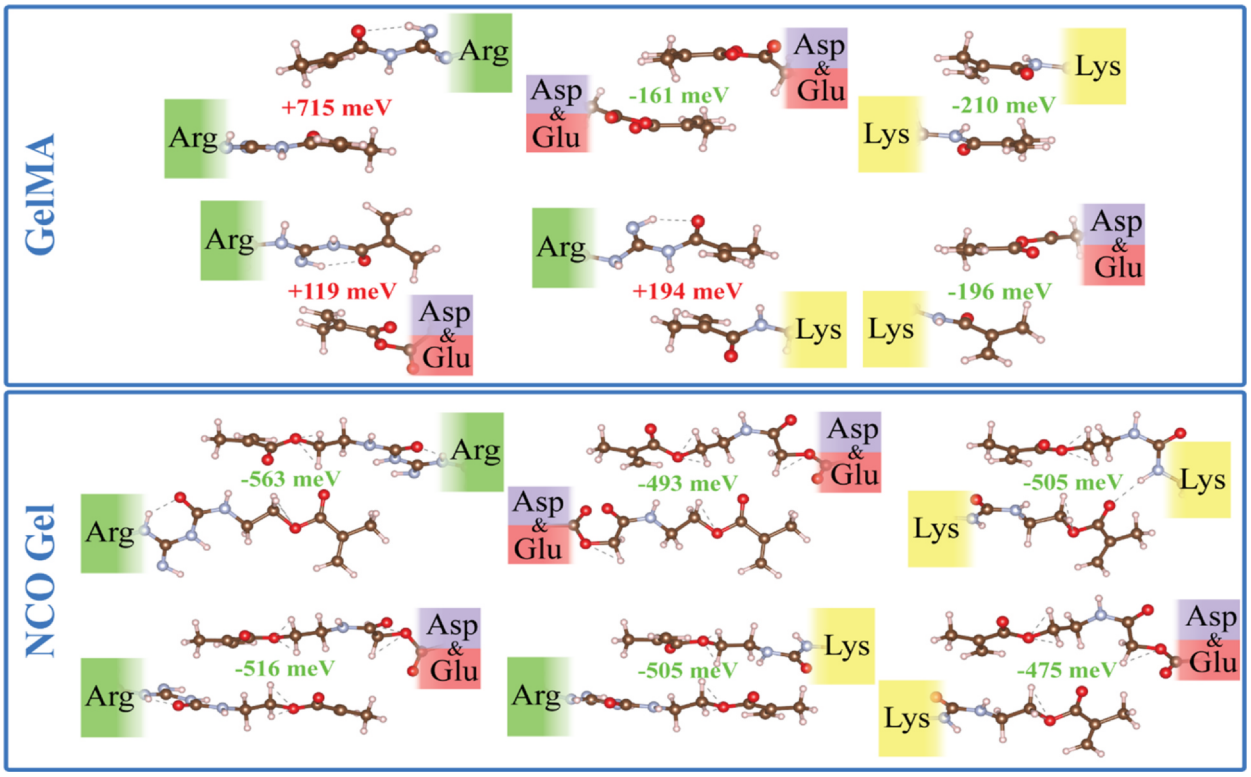

Fig. 1. The interaction energy profile of GelMA and NCO-Gel functional groups. Arg: arginine, Asp: aspartate, Glu: glutamate, Lys: lysine.

2.4. FTIR-ATR analysis

The lyophilized polymers were characterized using FTIR-ATR instruments with diamond/ZnSe crystal (Perkin Elmer-UATR TWO). The analysis was conducted between 650 and 4000 cm^{-1} wavenumber range with a resolution rate of 4 cm^{-1} and scan number of 20. The obtained data were plotted using graphing software OriginPro (Northampton, MA).

2.5. Dynamic light scattering analysis (DLS)

To figure out the physical and chemical gelation of the polymers, we investigated microrheology of NCO-Gel and GelMA polymers. During the analysis, the polymer solutions were analyzed at 30 °C to prevent physical gelation (GelMA and NCO-Gel polymers are known to form physical gels under 30 °C) and UV is applied to initiate the chemical crosslinking of vinyl bonds on the polymer backbone. The UV light (3 W, 365 nm) was applied sequentially and in very narrow intervals like 5, 10, and 20 s. After each curing the solution was analyzed again. The process was finished when polymer solutions get complete gelation. The raw correlation data was obtained and analyzed in graphing software OriginPro (Northampton, MA).

2.6. Biofabrication of the hydrogels

NCO-Gel and GelMA hydrogels were fabricated in a variety of ways. Polymers were dissolved in 1% Irgacure solution to final concentrations 5%, 7.5%, 10% and 15%(w/v) at 50 °C. To analyze the morphology and the swelling characteristics, hydrogels were produced in a 1 ml syringe. The syringe was put into UVP CL 1000 UV (365 nm) crosslinker cabin and cured until gelation. The hydrogels were ejected from the syringe and cut into small pieces. To observe moldability and complete gelation times of GelMA and NCO-Gel polymers, a molding technique was used. Molds were prepared from Polymethyl methacrylate (PMMA) with exact shapes like square, circle, star and honeycomb models. Polymer solutions (50 µl) were cast into the molds and UV (3 W, 365 nm led) cured until complete gelation. The gelation of NCO-Gel polymers is very fast and complete crosslinking in 10 s while GelMA gets gelation in 210 s. After gelation, hydrogels were removed from the molds. The hydrogels were examined in fluorescent microscopy. Also, the hydrogels were produced by bioprinting technique using Axolotl Biosystems Ltd. Axo A2 Bioprinting System. The NCO-Gel1 polymer solution was prepared at 5% (w/v) concentration and printed at 8 °C at 16.8 psi in 5 layers without pregelation. The printed construct was polymerized under UV light for maximum 10 s. 5% (w/v) GelMA2 hydrogel was printed at 25 psi and room temperature after 1.45 min UV cure for pregelation. After the printing process, GelMA2 hydrogel was crosslinked under 10 min UV cure. Although pregelation step is performed for all GelMA hydrogels (GelMA1, GelMA2 and GelMA3), only GelMA2 hydrogel was found to be printable therefore GelMA2 has been used for comparative studies.

2.7. Morphological analysis of hydrogels

To characterize morphology, hydrogels were frozen at −80 °C and freeze-dried after synthesis to remove water absorbed within a gel. The dried samples were cut into fragments, fixed on carbon bands and coated with a thin gold layer under argon gas (Emitech K550X). The samples were observed by scanning electron microscopy (FEI Quanta 250 FEG (Oregon, USA)) in varied magnifications. The pore size of the hydrogels was determined using ImageJ Software (NIH) by averaging data from at least 100 points on the surface.

2.8. Atomic force microscopy (AFM) analysis

AFM analysis was applied to determine elastic modulus of NCO-Gel and GelMA hydrogels at 5% (w/v). Hydrogels were formed as a very thin layer on a clean glass slide and dried in desiccator for 2 days and analyzed in NanosurfCoreAFM using contact mode tip with 0.2 N/m spring constant. The analysis was done using dried hydrogels due to the

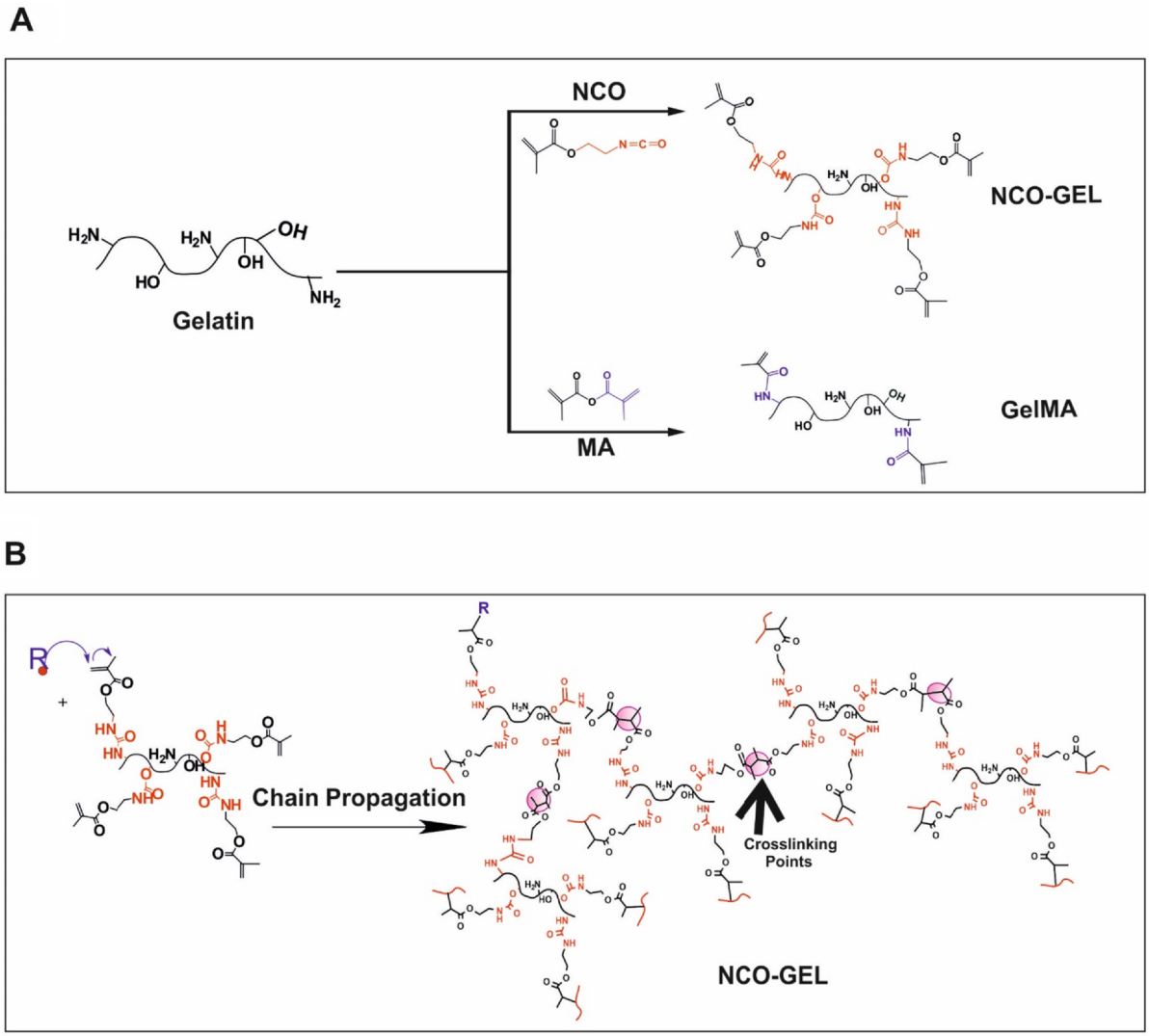

Fig. 2. Schematic representations of A) Modification of gelatin with Karenz and Methacrylic Anhydride to obtain NCO-Gel and GelMA polymers respectively. B) Crosslinking mechanism of NCO-Gel in the presence of Irgacure 2959 as photoinitiator.

Table 1
Compositions of synthesized NCO-Gel and GelMA polymers.

NCO-Gel	NCO(μl/1 g Gelatin)	GelMA	MA(μl/1 g Gelatin)
NCO-Gel1	74.6	GelMA1	100
NCO-Gel2	149.2	GelMA2	200
NCO-Gel3	268.6	GelMA3	400

difficulty of analysis of soft materials in AFM. Force-distance curves were obtained using raw data in the AtomicJ program. After analysis, we obtained Elastic modulus of dried hydrogels.

2.9. Cell culture and viability analysis

NIH 3T3 mouse fibroblast cells were cultured in high glucose DMEM containing L-glutamine and supplemented with 10% FBS and 1% penicillin/streptomycin. The cells were cultured up to ~90% confluency in a humidified environment (5% CO_2, 37 °C) and harvested cells were used for further cell viability studies. For Live/Dead and MTT assays, gels were conditioned with complete medium prior to cell seeding, and $1x10^4$ cells/well were used to evaluate cytotoxicity. Live/Dead and MTT assays were utilized to analyze cell viability and proliferation for long-term cultures (1/7/14/21 day) of NCO-Gel1, NCO-Gel3, GelMA1, GelMA2, and GelMA3 scaffolds. For Live/Dead analysis, CytoCalcein™ Green and PI were used in equal proportions after cell culture and cells were stained at 37 °C, 30 min. Then, visualization was performed using a fluorescence microscope (Zeiss Axio Observer). For MTT analysis reagent was added (5 mg mL^{-1}) to wells and incubated for 2–4 h followed by solubilizing formazan salt via DMSO. Measurements were carried out by Multiskan™ GO Microplate Spectrophotometer (Thermo Fisher Scientific). All data were evaluated as 4 replicates.

2.10. Theoretical calculations

In order to determine the structural properties and the interaction energies between the groups, density functional theory (DFT) calculations were carried out using Vienna *ab-initio* Simulation Package (VASP) with projector-augmented wave (PAW) potentials [38–41]. Generalized gradient approximation (GGA) was taken as the exchange-correlation functional. DFT-D3 method with Becke-Jonson damping was used in the van der Waals corrections [42]. As convergence criteria, total energy difference of 10^{-5} eV between consequent steps was taken. The kinetic energy cutoff of the plane-wave basis set was 400 eV in all total energy optimization calculations.

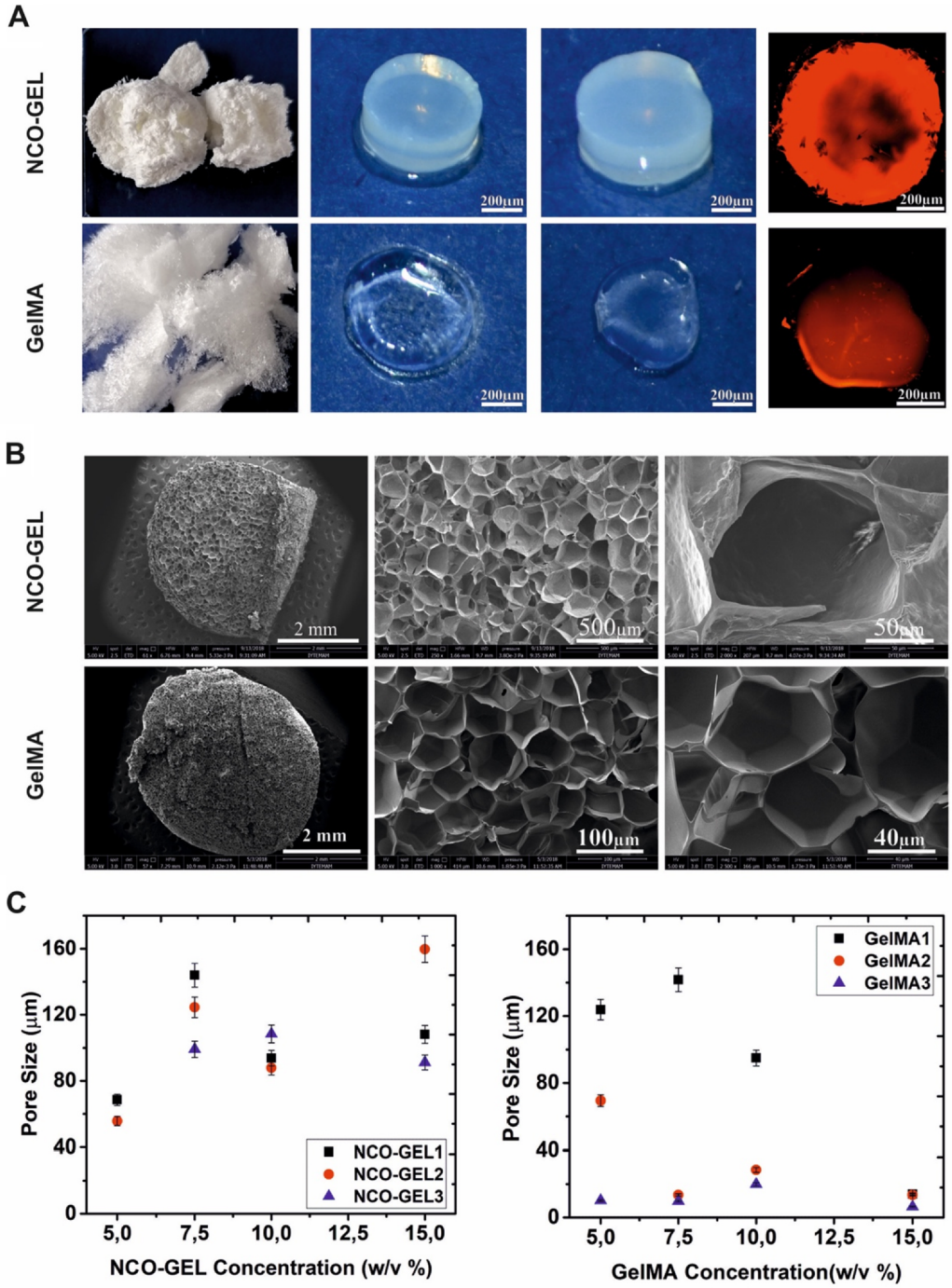

Fig. 3. Images of; A) Lyophilized polymers NCO-Gel and GelMA (first), NCO-Gel and GelMA hydrogels after synthesis (second) and after swelling of the hydrogels in water (third) and fluorescent images of the hydrogels after synthesis in mold (fourth). B) SEM images of lyophilized hydrogels of NCO-Gel and GelMA at different magnifications. C) Pore sizes of the hydrogels at different concentrations and hydrogel formulations.

3. Results and discussion

Here we propose that insertion of 2-isocyanatoethyl methacrylate group causes collective chain-chain interactions by its hydrogen bond donor acceptor character which promotes effective condensation of gelatin chains. In order to provide an atomic-level explanation to how the condensation is formed, we perform state of the art ab initio calculations. The interaction energy between hydrogen bonding pairs of 2-isocyanatoethyl methacrylate modified and methacrylic anhydride modified peptides is calculated according to the formula $E_{int} = E_{ab} - E_a - E_b$ where E_a (E_b) is the total energy of the isolated molecule and E_{ab} is the total energy of the molecules in interaction. Therefore, the attractive interaction between pairs takes place when $E_{int} < 0$. The interactions are found to be maximum in five different amino acid residues which are Arg-Arg, Lys-Lys, Asp-Asp, Glu-Glu and Lys-Asp/Glu by means of O—HN and N—OH hydrogen bonds. The interaction energy is calculated 475–563 meV for 2-isocyanatoethyl methacrylate modified gelatin whereas it is found to be 210 meV for methacrylic anhydride gelatin (Fig. 1). The 2-isocyanatoethyl methacrylate group insertion are considered to increase the interaction energy throughout the additional hydrogen bonding and therefore drives condensation of gelatin backbone to gel state.

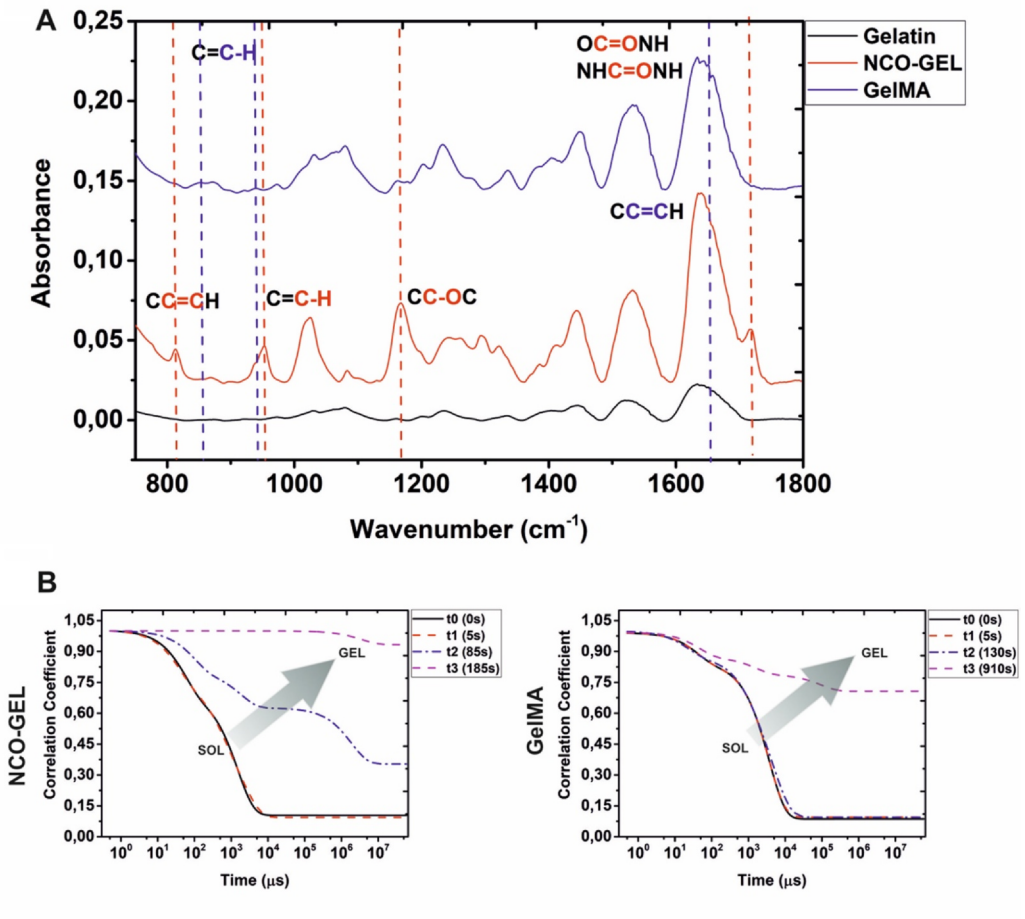

C

	UV Time(s)	τ1 (A1)	τ2 (A2)	τ3 (A3)
NCO-GEL	0	52,5 (0,30)	1523,6 (0,60)	- -
	5	35,9(0,24)	468,9 (0,25)	2382,9 (0,42)
	85	98,1 (0,19)	1841,5 (0,17)	1,89E6 (0,27)
	185		3,57E6 (0,99)	
GELMA	0	39,6 (0,14)	3719,49 (0,76)	- -
	5	39,1 (0,14)	3633,76 (0,75)	- -
	130	1175,3 (0,18)	22,52 (0,12)	5392,4 (0,59)
	910	46,06 (0,12)	1600,7 (0,085)	96294,4 (0,082)

Fig. 4. A) FT-IR spectra of pure Gelatin (black), NCO-Gel (red) and GelMA (blue). B) Correlograms of NCO-Gel and GelMA with different times of UV curing. C) Correlation equation data of NCO-Gel and GelMA with different times of UV curing, τ (μs) is relaxation time and A is percentage. (For interpretation of the references to colour in this figure legend, the reader is referred to the web version of this article.)

We anticipate that 2-isocyanatoethyl methacrylate group modulates hydrogen bonding pairs of gelatin and intensifies these interactions nearly three folds as compared to the commonly used methacrylic anhydride and therefore expediting assembly of macromolecular chains. Fig. 2A illustrates functionalization of Gelatin by two crosslinkers; 2-isocyanatoethyl methacrylate (NCO) and methacrylic anhydride (MA). As shown, GelMA contains solely amide groups whereas NCO-Gel contains urea and urethane groups on its backbone which is expected to drive rapid condensation of chains and gelation more effectively. Fig. 2B illustrates crosslinking of NCO-Gel bioink in the presence of the photoinitiator Irgacure 2959 by UV exposure (*Irgacure dissociates to radical precursors and attacks the double bonds of NCO-Gel that eventually generates gel*).

After, 2-isocyanatoethyl methacrylate (NCO) and methacrylic anhydride (MA) modification, gels were carefully separated from reaction medium and rinsed to eliminate unreacted chemicals then freeze-dried for easy handling in further processes. Images of lyophilized NCO-Gel and GelMA polymers are shown in Fig. 3A, and NCO-Gel exhibits foamy texture while GelMA is mostly in powder form. The dry residues of NCO-Gel and GelMA were dissolved in water then transferred in molds to conduct UV initiated crosslinking reaction which yielded hydrogels shown in Fig. 3A. When these hydrogels of NCO-Gel and GelMA were immersed in water, swelling occurred via water uptake. Here, the shape of NCO-Gel was found to be protected while GelMA lost its circular shape upon swelling. Moreover the fluorescent images of the hydrogels shown in Fig. 3A revealed that penetration of fluorescent dyes into NCO-Gel is in higher extent as compared to GelMA. These results refer that NCO-Gel is firm but might be made of interconnected domains therefore provide free diffusion of small molecules in hydrogel structure whereas GelMA exhibits loose hydrogel properties beacuse of lack of extra hydrogen bonding. Fluorescent image of GelMA hydrogel may be evidence of its lesser interconnectivity which limits the free diffusion. The SEM images shown in Fig. 3B give an idea about morphologies of the dried NCO-Gel and GelMA. As seen, both materials have porous surface however pore sizes were found to be relatively higher in NCO-Gel (40 to 160 μm) as compared to GelMA (20 to 120 μm). In general,

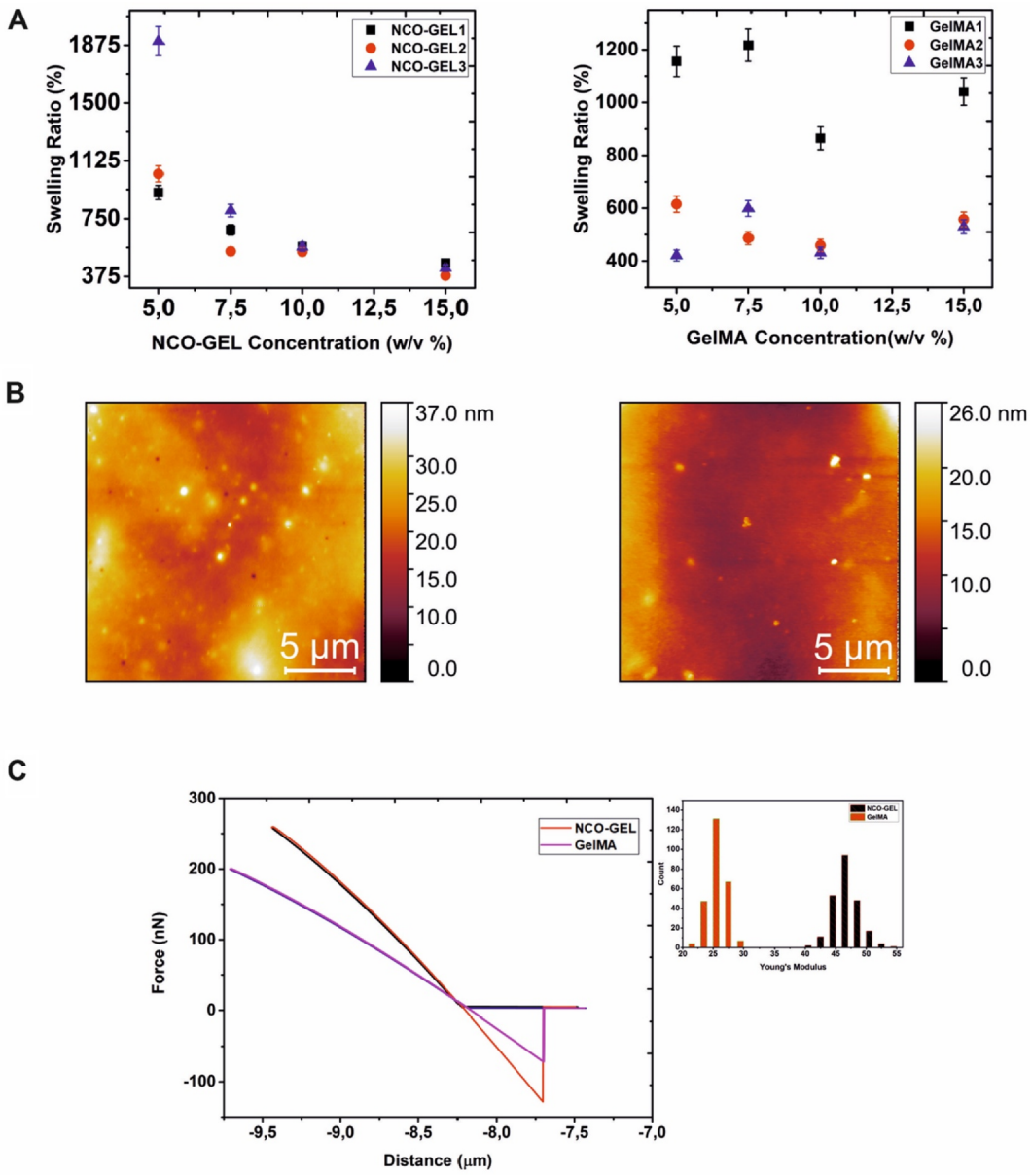

Fig. 5. A) Percent swelling ratios of NCO-Gel and GelMA hydrogels in water. B) Topographic AFM image of NCO-Gel (left) and GelMA (right) C) Young's modulus distributions and Force Distance curves of NCO-Gel and GelMA hydrogels.

GelMA exhibits smaller pores sizes as compared to NCO-Gel. The Fig. 3C summarizes the pore size variation for increasing initial gel content. As seen in Fig. 3C increasing gel content increases pore size for NCO-Gel while no clear trend observed for GelMA except pore size of GelMA hydrogels decreases as the methacrylation degree of gelatin increases regardless of the polymer concentration. In general, the pore size of both hydrogels were not found to be controlled by variation of initial concentrations.

The Fig. 4A shows IR spectra of NCO-Gel (red traces) and GelMA (blue traces), displaying characteristic bands of 3500, 2900 and 1650 cm^{-1} that correspond to O—H, C—H, C═O stretches respectively. The peaks at 1633, 1540 and 1237 cm^{-1} were assigned to the C═O stretching vibrations of the amide group, N—H bending vibrations of amide (II) and N—H bending of amide (III). C—H stretching gives signals at 953 and 943, 853 cm^{-1} for NCO-Gel and GelMA respectively. The very sharp difference between spectra of GelMA and NCO-gel is the peak at 1718 cm^{-1} that refers to intermolecular hydrogen bonding of urea/urethane groups. As discussed by Eckes et al. the peaks at 1710–1720 cm^{-1} refer to self-organization of chains via intermolecular hydrogen bonding in peptides. Martin et al. has also reported similar observation for peaks at 1690–1720 cm^{-1} corresponds to hydrogen bonding in gels [43,44]. These results assure that NCO-Gel is able to facilitate intermolecular hydrogen bonding through urea and urethane moieties as compared to GelMA. Other distinctive feature of the NCO-Gel spectra was the peak at 1166 cm^{-1} refers to C—O ether stretching in ether bond (C—O—C) which was typical for urethanes. Here urea and urethane groups are foreseen to increase hydrogen bonding between chains thereby increasing the interchain interactions as well as chain condensation which might significantly expedite gelation. This assumption has been tested by monitoring the gelation time. Fig. 4B shows DLS analysis results of NCO-Gel and GelMA polymers while chemical gelation under UV light. The DLS analysis showed that the transition from sol to gel phase via UV curing is faster in NCO-Gel than GelMA. In Fig. 4C, correlation equation data of NCO-Gel and GelMA with different times of UV curing has shown here τ (μs) is relaxation time and A is weighted percentage. Prior to UV triggered gelation process, both NCO-Gel and GelMA exhibited bimodal τ distributions (NCO-Gel = τ_1: 52.5 μs, τ_2: 1523.6 μs and GelMA = τ_1: 39.6 μs, τ_2:

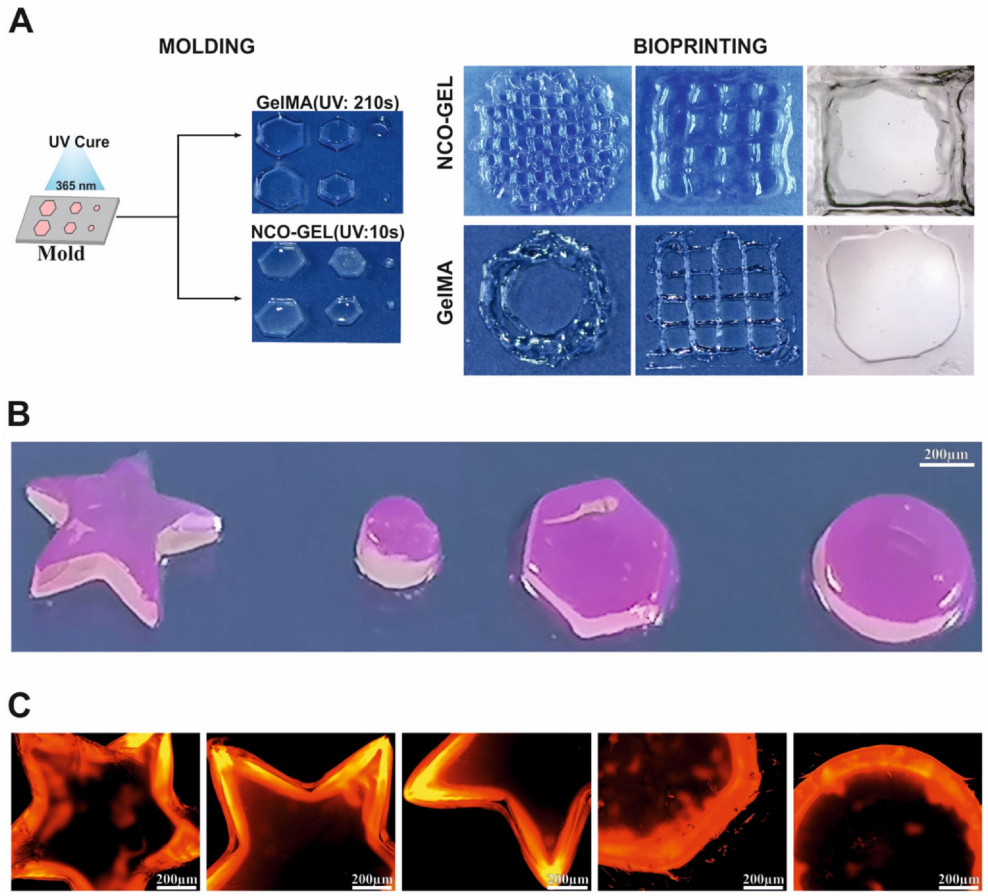

Fig. 6. A) Molding and BioPrinting of NCO-Gel and GelMA hydrogels fabricated at different shapes, B) Large size molding of NCO-Gel in different geometries. C) Fluorescent images of fabricated NCO-Gel hydrogels. Scale bars: 200 μm, the hydrogels are stained with Rhodamine during gelation.

3719.5 μs) indicating that more than one species were exist. The five second curing process has triggered formation of large sized assembly with τ_1: 2382.9 μs whereas GelMA exhibited no substantial change. This indicates gelation already started for NCO-Gel while GelMA is at still solution state. DLS analysis showed that the longer the UV curing the larger the size of the objects for both NCO-Gel and GelMA. However NCO-Gel has showed monomodal τ distribution which corresponds to interconnected single object whereas GelMA still shows three relaxation time components after 900 s curing. We concluded that NCO-Gel exhibits faster gelation process than GelMA.

In next step we have studied the swelling capabilities of the hydrogels given in percent swelling ratio (SR %) graph versus hydrogel concentration (Fig. 5A). %SR of the NCO-Gel hydrogels show a downward pattern from NCO-Gel3 to NCO-Gel1. In the NCO-Gel backbone, the number of amino groups rises after modification of gelatin with 2-isocyanatoethyl methacrylate (see Fig. 2A). Since the swelling of the hydrogels occurs via capture of H^+ by amino groups, swelling ability of NCO-Gel hydrogels with higher modification rises from NCO-Gel1 to NCO-Gel3. As an example, NCO-Gel3 has nearly 1900% while NCO-Gel2 and NCO-Gel1 have nearly 1100% and 900% swelling ratio respectively in 5% (w/v) polymer concentration. In addition, swelling ability of NCO-Gel hydrogels declines when polymer concentration increases. For instance, NCO-Gel1 hydrogels have nearly 918%, 676%, 568% and 461% swelling ratios in 5, 7.5, 10 and 15% (w/v) polymer concentrations respectively. NCO-Gel2 and NCO-Gel3 hydrogels follow the same decreasing trend in swelling capacity in response to increasing polymer concentration. As seen, %SR decreases from GelMA1 to GelMA3 in all GelMA concentrations due to increasing methacrylation degrees. This trend in %SR is reverse of that of NCO-Gel hydrogels. Methacrylation of gelatin proceeds through NH_2 groups on gelatin backbone so the increasing MA on backbone decreases free amino groups. Amino groups are able to capture H^+ and polymer chains get far from each other, absorbing water into the gap between polymer chains and hydrogel swells in water. For example in 5% (w/v) polymer concentration, GelMA1, GelMA2 and GelMA3 has nearly 1155%, 615% and 421% swelling capacities respectively. This decreasing trend is also seen in 7.5%, 10% and 15% polymer concentrations. As clearly seen from the graph, methacrylation decreases the swelling ability of GelMA hydrogel whereas polymer concentration in hydrogel affects swelling ratio positively. In GelMA1, swelling ratio decreases from 1155% to 1041% when polymer concentration increases from 5% to 15% (w/v). In GelMA2, 5% (w/v) gel has nearly 615% and 15% gel has nearly 557% swelling ratio. The same trend can be seen in all GelMA concentrations except some deviations in swelling ratio. The Fig. 5B and show AFM imaging of both gels on solid substrate. Gels shows no distinct topographical features. The adhesion map shown in Fig. 5C shows nanomechanical analysis of both GelMA and NCO-Gel, in which NCO-Gel has steeper slope in force distance curve as compared to GelMA gel. Kuhori et. al has recently discussed significant changes in stiffness of gel-polyelectrolyte composites by characterizaiton of slope of force-distance curves [45]. As described, steeper slopes refer to stiffer gels. Therefore, we also concluded that slight upward change in slope of force-distance curve refers to deformation is lesser extent in NCO-Gel as compared to GelMA. This may be attributed to the increase in hydrogen bonding in NCO-Gel. Therefore comparison to GelMA hydrogels, NCO-Gel was found to be slightly stiffer [46,47].

The biofabrication of hydrogels is done using molding and bioprinting techniques as shown in Fig. 6A. PMMA mold is prepared with honeycomb shape and a pregel solution is immersed into the mold following UV cure is applied for crosslinking. The solution mixtures of

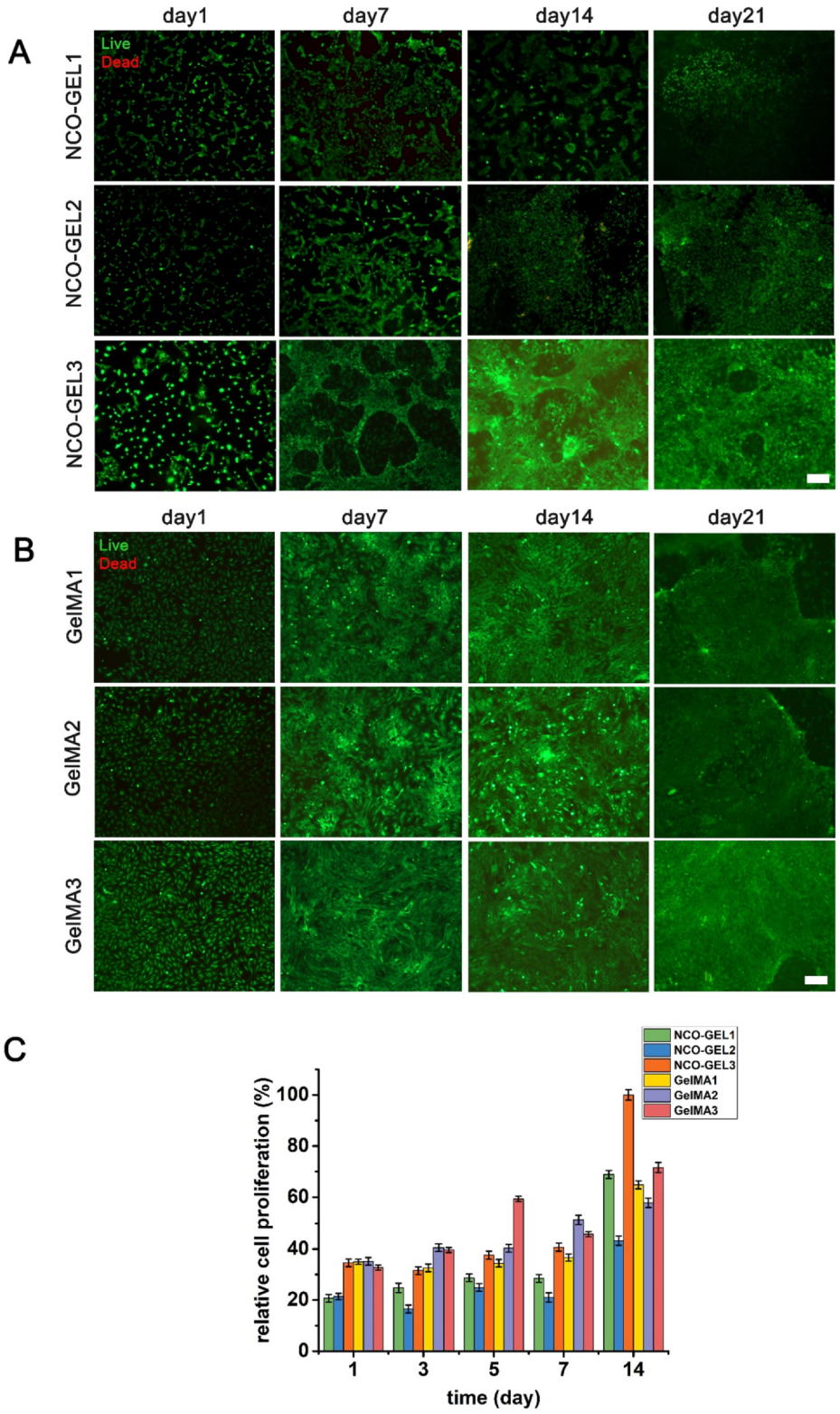

Fig. 7. NIH 3T3 cell proliferation and viability profiles evaluated by; A) Live-dead analysis of NCO-Gel1, NCO-Gel2 and NCO-Gel3 for day1, 7, 14 and 21 (Scale bar: 200 μm), B) Live-dead analysis of GelMA1, GelMA2 and GelMA2 for day1, 7, 14 and 21 (Scale bar: 200 μm), C) Cell proliferation via MTT assay of 3D cultured cells on NCO-Gel1, NCO-Gel2, NCO-Gel3, GelMA1, GelMA2, and GelMA3 for 14 days (n = 4).

NCO-Gel and GelMA have been exposed to UV radiation till no fluid content remains and gelation times were found to be 10 and 210 s for NCO-Gel and GelMA respectively. These results indicate that NCO modified gelatin is readily transformed to the gel state by the NCO molecule has an accelerating effect of NCO molecule on chain condensation. The most significant features of NCO-Gels are fast gelation, rigid features and also being easy to shape. Molded hexagon shape gels made of NCO-Gel have sharp, homogenous edges as compared to GelMA made gels. Moreover, during bioprinting method, NCO-Gel polymer protects its shape after being printed onto substrate while

GelMA polymer spreads on substrate so it cannot protect printed shape exactly. To exemplify a large scale biofabrication application we showed the moldability of NCO-Gel hydrogels, the hydrogels are molded at different shapes as shown in Fig. 6B. The hydrogels are stained with Rhodamine during gelation. The hydrogel takes the shape of mold easily and without any defect in its soft structure. Fig. 6C shows fluorescent images of molded NCO-Gel hydrogels. As seen, the details and corners of shapes like in star models are very clear and the hydrogel protects the shape for a long time in air and in water. The resultant gel in various geometries preserve their integrity throughout overall stiffness of NCO-Gel which is provided by stronger intermolecular hydrogen bonding.

To evaluate the cell proliferation, viability and toxicity, MTT and live-dead analyses were done via culturing NIH 3T3 fibroblast cells on varied formulations of 3D NCO-Gels. For comparison, similar formulations of GelMA hydrogels were used. Cell viability and proliferation profiles were investigated via live-dead assay as shown in Fig. 7. As given in Fig. 7A, rapid and homogeneous cell adhesion, and cell proliferation was observed on day1 for all formulations of NCO-Gel. Highest cell proliferation and viability was observed for NCO-Gel3 while NCO-Gel1 and NCO-Gel2 had lower cell proliferation and viability profiles for long-term culturing up to day 21. Later cell viability and proliferation results were also supported by MTT analysis (Fig. 7C). Increasing cell proliferation was observed for all NCO-Gel during 14-day cell culturing. For NCO-Gel3, cell proliferation increased 65% from day 1 to day 14, while it was 50% and 25% increase for NCO-Gel1 and NCO-Gel2, respectively. In parallel with live-dead analysis results, NCO-Gel3 showed the highest cell proliferation and viability on day 14 compared to both NCO-Gel counterparts and GelMA controls. We have showed that, newly formulated NCO-Gels were compared with GelMA in terms of cell adhesion, proliferation and cell viability, since GelMA is a well-known and well-characterized scaffold that had been used for tissue engineering studies due to its biocompatible property and tunable physical characteristic [48–51]. The results emphasize that NCO-Gel3 favors cellular adhesion which has led to higher cell proliferation. Also, porous structure and interconnected pores of NCO-Gel3 allows infiltration of cells to inner layers, which supports 3D cell culture formation. Moreover, that results support that particularly NCO-Gel hydrogels would be suitable candidates as scaffold for tissue engineering studies.

4. Conclusion

We have shown the synthesis of 2-isocyanatoethyl methacrylate (NCO)modified gelatin that providing printable and biocompatible ink for bioprinting applications. Our theoretical calculations demonstrated that insertion of 2-isocyanatoethyl methacrylate doubles the interaction energy (500 meV) between gelatin chains providing significant contribution in interchain condensation and self-organization as compared to methacrylic anhydride modified gelatin (GelMA). The NCO-Gel was found to be more firm and mechanically strong that provides advantages in molding as well as bioprinting processes. Bioprinted NCO-Gel has shown sharp borders and stable 3D geometry as compared to GelMA ink under 10 s UV curing time. The cell viability tests confirm that NCO-Gel facilitates cell proliferation and supports cell viability. We foresee that NCO-Gel bioink formulation provides a promising opportunity when low dose UV curing and rapid printing are required.

5. Data availability statement

The raw/processed data required to reproduce these findings cannot be shared at this time due to legal or ethical reasons.

Declaration of Competing Interest

The authors declare that they have no known competing financial interests or personal relationships that could have appeared to influence the work reported in this paper.

Acknowledgements

This study has been supported by the IZTECH-Scientific Research Project (2020-İYTE-0060).

The SEM micrographs were obtained at Material Research Center İYTE (IZTECH-MAM).

Author Buşra Koksal and Rabia Onbas are TUBİTAK 2211-A scholarship holders.

We are thankful to Axolotl Biosystems Ltd and Can Garipoğlu for their continuous technical support.

References

[1] A. Koroleva, A. Deiwick, A. Nguyen, R. Narayan, A. Shpichka, O. Kufelt, R. Kiyan, V. Bagratashvili, P. Timashev, T. Scheper, B. Chichkov, Hydrogel-based microfluidics for vascular tissue engineering, BioNanoMaterials 17 (1–2) (2016).
[2] R.M. Costa, S. Rauf, C.A.E. Hauser, Towards biologically relevant synthetic designer matrices in 3D bioprinting for tissue engineering and regenerative medicine, Curr. Opin. Biomed. Eng. 2 (2017) 90–98.
[3] S. van Kogelenberg, Z. Yue, J.N. Dinoro, C.S. Baker, G.G. Wallace, Three-dimensional printing and cell therapy for wound repair, Adv. Wound Care (New Rochelle) 7 (5) (2018) 145–155.
[4] S. Adepu, N. Dhiman, A. Laha, C.S. Sharma, S. Ramakrishna, M. Khandelwal, Three-dimensional bioprinting for bone tissue regeneration, Curr. Opin. Biomed. Eng. 2 (2017) 22–28.
[5] W. Wei, J. Li, X. Qi, Y. Zhong, G. Zuo, X. Pan, T. Su, J. Zhang, W. Dong, Synthesis and characterization of a multi-sensitive polysaccharide hydrogel for drug delivery, CarbohydrPolym 177 (2017) 275–283.
[6] M.L. Lovett, X. Wang, T. Yucel, L. York, M. Keirstead, L. Haggerty, D.L. Kaplan, Silk hydrogels for sustained ocular delivery of anti-vascular endothelial growth factor (anti-VEGF) therapeutics, Eur. J. Pharm. Biopharm. 95 (Pt B) (2015) 271–278.
[7] H.Q. Wu, C.C. Wang, Biodegradable smart nanogels: a new platform for targeting drug delivery and biomedical diagnostics, Langmuir 32 (25) (2016) 6211–6225.
[8] S.L. Lim, C.-W. Ooi, W.S. Tan, E.-S. Chan, K.L. Ho, B.T. Tey, Biosensing of hepatitis B antigen with poly(acrylic acid) hydrogel immobilized with antigens and antibodies, Sens. Actuators, B 252 (2017) 409–417.
[9] N.A. Peppas, D.S. Van Blarcom, Hydrogel-based biosensors and sensing devices for drug delivery, J. Control Release 240 (2016) 142–150.
[10] I.Y. Jung, J.S. Kim, B.R. Choi, K. Lee, H. Lee, Hydrogel based biosensors for in vitro diagnostics of biochemicals, proteins, and genes, Adv. Healthc. Mater. 6 (12) (2017).
[11] W. Wu, S. Zhou, Hybrid micro-/nanogels for optical sensing and intracellular imaging, Nano Rev. 1 (2010).
[12] M. Chan, J. Lux, T. Nishimura, K. Akiyoshi, A. Almutairi, Long-lasting and efficient tumor imaging using a high relaxivity polysaccharide nanogel magnetic resonance imaging contrast agent, Biomacromolecules 16 (9) (2015) 2964–2971.
[13] W. Wu, J. Shen, P. Banerjee, S. Zhou, Core-shell hybrid nanogels for integration of optical temperature-sensing, targeted tumor cell imaging, and combined chemo-photothermal treatment, Biomaterials 31 (29) (2010) 7555–7566.
[14] A. Arslan-Yildiz, R. El Assal, P. Chen, S. Guven, F. Inci, U. Demirci, Towards artificial tissue models: past, present, and future of 3D bioprinting, Biofabrication 8 (1) (2016) 014103.
[15] H. Cheng, R. Chabok, X. Guan, A. Chawla, Y. Li, A. Khademhosseini, H.L. Jang, Synergistic interplay between the two major bone minerals, hydroxyapatite and whitlockite nanoparticles, for osteogenic differentiation of mesenchymal stem cells, Acta Biomater. 69 (2018) 342–351.
[16] B.J. Klotz, D. Gawlitta, A. Rosenberg, J. Malda, F.P.W. Melchels, Gelatin-methacryloyl hydrogels: towards biofabrication-based tissue repair, Trends Biotechnol. 34 (5) (2016) 394–407.
[17] B. Yildiz, S. Ozenler, M. Yucel, U.H. Yildiz, A. Arslan Yildiz, Biomimetic and synthetic gels for nanopharmaceutical applications, in: V.K. Yata, S. Ranjan, N. Dasgupta, E. Lichtfouse (Eds.), Nanopharmaceuticals: Principles and Applications, vol. 1, Springer International Publishing, Cham, 2021, pp. 273–309.
[18] A. Skardal, A. Atala, Biomaterials for integration with 3-D bioprinting, Ann. Biomed. Eng. 43 (3) (2015) 730–746.
[19] P. Chandra, A. Atala, Engineering blood vessels and vascularized tissues: technology trends and potential clinical applications, Clin. Sci. 133 (9) (2019) 1115–1135.
[20] Q. Gu, E. Tomaskovic-Crook, R. Lozano, Y. Chen, R.M. Kapsa, Q. Zhou, G.G. Wallace, J.M. Crook, Functional 3D neural mini-tissues from printed gel-based bioink and human neural stem cells, Adv. Healthcare Mater. 5 (12) (2016) 1429–1438.
[21] W. Jia, P.S. Gungor-Ozkerim, Y.S. Zhang, K. Yue, K. Zhu, W. Liu, Q. Pi, B. Byambaa, M.R. Dokmeci, S.R. Shin, A. Khademhosseini, Direct 3D bioprinting of perfusable vascular constructs using a blend bioink, Biomaterials 106 (2016) 58–68.

[22] C. Chong, Z. Ming-liang, Z. Ren-kun, L. Gang, Z. Chang-yu, F. Feng, S. Hong-tao, Z. Sai, T. Yue, L. Xiao-hong, Collagen/heparin sulfate scaffolds fabricated by a 3D bioprinter improved mechanical properties and neurological function after spinal cord injury in rats, J. Biomed. Mater. Res. Part A 105 (5) (2017) 1324–1332.
[23] K. Yue, G. Trujillo-de Santiago, M.M. Alvarez, A. Tamayol, N. Annabi, A. Khademhosseini, Synthesis, properties, and biomedical applications of gelatinmethacryloyl (GelMA) hydrogels, Biomaterials 73 (2015) 254–271.
[24] I. Cicha, R. Detsch, R. Singh, S. Reakasame, C. Alexiou, A.R. Boccaccini, Biofabrication of vessel grafts based on natural hydrogels, Curr. Opin. Biomed. Eng. 2 (2017) 83–89.
[25] L.E. Bertassoni, J.C. Cardoso, V. Manoharan, A.L. Cristino, N.S. Bhise, W.A. Araujo, P. Zorlutuna, N.E. Vrana, A.M. Ghaemmaghami, M.R. Dokmeci, A. Khademhosseini, Direct-write bioprinting of cell-laden methacrylatedgelatin hydrogels, Biofabrication 6 (2) (2014) 024105.
[26] A. Skardal, J. Zhang, L. McCoard, X. Xu, S. Oottamasathien, G.D. Prestwich, Photocrosslinkable hyaluronan-gelatin hydrogels for two-step bioprinting, Tissue Eng. Part A 16 (8) (2010) 2675–2685.
[27] S.R. Shin, R. Farzad, A. Tamayol, V. Manoharan, P. Mostafalu, Y.S. Zhang, M. Akbari, S.M. Jung, D. Kim, M. Comotto, N. Annabi, F.E. Al-Hazmi, M.R. Dokmeci, A. Khademhosseini, A bioactive carbon nanotube-based ink for printing 2D and 3D flexible electronics, Adv. Mater. 28 (17) (2016) 3280–3289.
[28] A. Skardal, D. Mack, E. Kapetanovic, A. Atala, J.D. Jackson, J. Yoo, S. Soker, Bioprinted amniotic fluid-derived stem cells accelerate healing of large skin wounds, Stem Cells Transl. Med. 1 (11) (2012) 792–802.
[29] H.W. Kang, S.J. Lee, I.K. Ko, C. Kengla, J.J. Yoo, A. Atala, A 3D bioprinting system to produce human-scale tissue constructs with structural integrity, Nat. Biotechnol. 34 (3) (2016) 312–319.
[30] J. Yin, M. Yan, Y. Wang, J. Fu, H. Suo, 3D bioprinting of low-concentration cell-laden gelatin methacrylate (GelMA) bioinks with a two-step cross-linking strategy, ACS Appl. Mater. Interfaces 10 (8) (2018) 6849–6857.
[31] R. Levato, W.R. Webb, I.A. Otto, A. Mensinga, Y. Zhang, M. van Rijen, R. van Weeren, I.M. Khan, J. Malda, The bio in the ink: cartilage regeneration with bioprintable hydrogels and articular cartilage-derived progenitor cells, Acta Biomater. 61 (2017) 41–53.
[32] T. Billiet, B.V. Gasse, E. Gevaert, M. Cornelissen, J.C. Martins, P. Dubruel, Quantitative contrasts in the photopolymerization of acrylamide and methacrylamide-functionalized gelatin hydrogel building blocks, Macromol. Biosci. 13 (11) (2013) 1531–1545.
[33] S.V. Vlierberghe, E. Schacht, P. Dubruel, Reversible gelatin-based hydrogels: fine-tuning of material properties, Eur. Polym. J. 47 (5) (2011) 1039–1047.
[34] I. Van Nieuwenhove, B. Stubbe, G.-J. Graulus, S. Van Vlierberghe, P. Dubruel, Protein functionalization revised: N-tert-butoxycarbonylation as an elegant tool to circumvent protein crosslinking, Macromol. Rapid Commun. 35 (15) (2014) 1351–1355.
[35] H.H. Kim, J.W. Kim, J. Choi, Y.H. Park, C.S. Ki, Characterization of silk hydrogel formed with hydrolyzed silk fibroin-methacrylate via photopolymerization, Polymer 153 (2018) 232–240.
[36] K. Jung, N. Corrigan, M. Ciftci, J. Xu, S.E. Seo, C.J. Hawker, C. Boyer, Designing with light: advanced 2D, 3D, and 4D materials, Adv. Mater. 32 (2020) 1903850.
[37] M. Eslami, N.E. Vrana, P. Zorlutuna, S. Sant, S. Jung, N. Masoumi, R.A. Khavari-Nejad, G. Javadi, A. Khademhosseini, Fiber-reinforced hydrogel scaffolds for heart valve tissue engineering, J. Biomater. Appl. 29 (3) (2014) 399–410.
[38] G. Kresse, J. Hafner, Ab initio molecular dynamics for liquid metals, Phys. Rev. B 47 (1) (1993) 558.
[39] G. Kresse, J. Furthmüller, Efficient iterative schemes for ab initio total-energy calculations using a plane-wave basis set, Phys. Rev. B 54 (16) (1996) 11169.
[40] P.E. Blöchl, Projector augmented-wave method, Phys. Rev. B 50 (24) (1994) 17953.
[41] J.P. Perdew, K. Burke, M. Ernzerhof, Generalized gradient approximation made simple, Phys. Rev. Lett. 77 (18) (1996) 3865.
[42] S. Grimme, S. Ehrlich, L. Goerigk, Effect of the damping function in dispersion corrected density functional theory, J. Comput. Chem. 32 (7) (2011) 1456–1465.
[43] K.M. Eckes, X. Mu, M.A. Ruehle, P. Ren, L.J. Suggs, β sheets not required: combined experimental and computational studies of self-assembly and gelation of the ester-containing analogue of an Fmoc-dipeptide hydrogelator, Langmuir 30 (18) (2014) 5287–5296.
[44] A.D. Martin, J.P. Wojciechowski, H. Warren, M. Panhuis, P. Thordarson, Effect of heterocyclic capping groups on the self-assembly of a dipeptide hydrogel, Soft Matter 12(10) (2016) 2700–2707.
[45] L.R. Khoury, I. Popa, Chemical unfolding of protein domains induces shape change in programmed protein hydrogels, Nat. Commun. 10 (2019) 5439.
[46] S. Ahadian, J. Ramón-Azcón, M. Estili, X. Liang, S. Ostrovidov, H. Shiku, M. Ramalingam, K. Nakajima, Y. Sakka, H. Bae, T. Matsue, A. Khademhosseini, Hybrid hydrogels containing vertically aligned carbon nanotubes with anisotropic electrical conductivity for muscle myofiber fabrication, Sci. Rep. 4 (1) (2014) 4271.
[47] A. Navaei, H. Saini, W. Christenson, R.T. Sullivan, R. Ros, M. Nikkhah, Gold nanorod-incorporated gelatin-based conductive hydrogels for engineering cardiac tissue constructs, Acta Biomater. 41 (2016) 133–146.
[48] J.W. Nichol, S.T. Koshy, H. Bae, C.M. Hwang, S. Yamanlar, A. Khademhosseini, Cell-laden microengineered gelatin methacrylate hydrogels, Biomaterials 31 (21) (2010) 5536–5544.
[49] X. Zhao, Q. Lang, L. Yildirimer, Z.Y. Lin, W. Cui, N. Annabi, K.W. Ng, M.R. Dokmeci, A.M. Ghaemmaghami, A. Khademhosseini, PhotocrosslinkableGelatin hydrogel for epidermal tissue engineering, Adv. Healthc. Mater. 5 (1) (2016) 108–118.
[50] J. Lee, G. Kim, A cryopreservable cell-laden GelMa-based scaffold fabricated using a 3D printing process supplemented with an in situ photo-crosslinking, J. Ind. Eng. Chem. 85 (2020) 249–257.
[51] H. Rastin, R.T. Ormsby, G.J. Atkins, D. Losic, 3D bioprinting of methylcellulose/gelatin-methacryloyl (MC/GelMA) bioink with high shape integrity, ACS Appl. Bio Mater. 3 (3) (2020) 1815–1826.